

# Electrogram Fractionation Caused by Microfibrosis: Insights from a Microstructure Model

V Jacquemet, B Robinson, CS Henriquez

Duke University, Durham, NC, USA

## Abstract

*Fractionated electrograms have long been associated with non-uniform propagation in the atria, owing to a heterogeneous substrate marked by fibrosis. It is not known, however, whether the features of the electrograms can be used to quantify the degree of fibrosis in the heart. A computer model of a monolayer of cells was developed to investigate how progression of microfibrosis impacts electrogram morphology and the degree of fractionation. The analysis of unipolar electrograms simulated in the model revealed that more pronounced microfibrosis was associated with slow conduction and electrogram waveforms featuring a higher degree of fractionation and a larger spatial variability in morphology. This modeling framework forms a basis to better understand the genesis of fractionated electrograms and for developing a strategy to use the electrogram features to quantify fibrosis in patients with atrial fibrillation, possibly impacting the target sites for catheter ablation.*

## 1. Introduction

Complex fractionated atrial electrograms are currently used as potential targets for catheter ablation therapy of atrial fibrillation [1]. Although fibrosis has been associated with the presence of fractionated electrograms, characterizing the substrate through the inspection of these signals is challenging. As a result, it is still unclear whether the severity of fibrosis can be revealed by analyzing electrograms. The purpose of this study is to develop a computational framework to determine how progression of microfibrosis leads to changes in electrogram morphology.

## 2. Methods

### 2.1. Microstructure model

Following the approach proposed by Spach *et al.* [2], a two-dimensional model representing the microstructure of

a monolayer cardiac tissue, 8.64 by 2.88 mm in size, was created, as described in Jacquemet *et al.* [3]. The model was composed of 8,354 randomly shaped cells (length:  $156 \pm 29 \mu\text{m}$ ; cross-section:  $213 \pm 75 \mu\text{m}^2$ ) generated using a technique similar to that of Hubbard *et al.* [4]. The myocytes were discretized into segments of size 15 by 10  $\mu\text{m}$ . The myocyte membrane kinetics was described by the Ramirez *et al.* model of canine atrial cell [5], with the sodium channel conductance increased by 50% [2,3].

Discrete cell-to-cell coupling was introduced to reproduce the gap junction distribution observed in adult cardiac tissue (Fig. 1). These electrical connections were mainly located at end-to-end regions (intercalated disk). Additional sparse coupling covering 30% of the remaining cell lateral wall was added [3]. The coupling conductance per unit contact area between the connected cell segments was set to  $8.182 \text{ nS}/\mu\text{m}^2$  for both longitudinal and transverse connections [3]. The resistivity of the intracellular medium was assumed to be  $200 \Omega \text{ cm}$ .

Microfibrosis was introduced as a set of collagenous septa disconnecting transverse coupling [2]. These septa were aligned with fiber orientation and randomly distributed over the tissue, covering 10%, 20% or 30% of the side-to-side contact area between the myocytes (microfibrosis density  $D$ ), and having an average length ( $L$ ) of 165  $\mu\text{m}$ , 315  $\mu\text{m}$ , 630  $\mu\text{m}$  or 945  $\mu\text{m}$ . For each of the 12 cases, 6 different realizations of the random distribution were generated. Examples of microfibrosis distribution are shown in Fig. 1.

Electrical propagation was simulated in the mono-domain framework using the CardioWave package (<http://cardiowave.duke.edu>). Transverse plane waves were initiated by stimulating an edge of the rectangular tissue. Conduction velocity (CV) was computed by linear regression of the activation times. Unipolar electrograms were computed using the current source approximation [6] at 87 sites forming an ellipse-shaped grid of electrodes. The signals were scaled so that the average peak-to-peak amplitude was 10 mV in the absence of microfibrosis (control case).

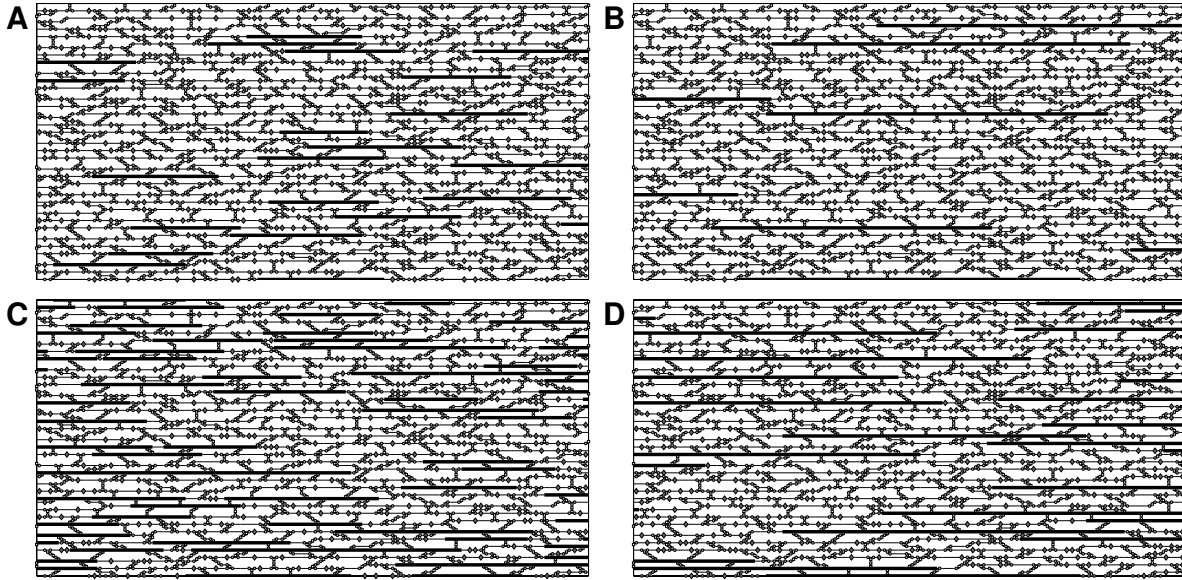


Figure 1. Microstructural models with microfibrosis characterized by different density ( $D$ ) and average length ( $L$ ) of microfibrosis. Zoom on a  $1.5 \times 0.75$  mm piece of tissue. Gap junctions are shown as circles (intercalated disk) or diamonds (transverse coupling) and collagen septa as thick horizontal lines. (A)  $L = 315 \mu\text{m}$ ,  $D = 10\%$ ; (B)  $L = 945 \mu\text{m}$ ,  $D = 10\%$ ; (C)  $L = 315 \mu\text{m}$ ,  $D = 30\%$ ; (D)  $L = 945 \mu\text{m}$ ,  $D = 30\%$ .

## 2.2. Signal analysis

Electrogram morphology was characterized by its amplitude, its asymmetry and its number of deflections. The absolute value of the maximal and minimal voltage in the electrogram complex was denoted by  $R$  and  $S$ . The amplitude  $A$  and the asymmetry  $a$  of an electrogram waveform were defined as [6, 7]:

$$A = R + S \quad \text{and} \quad a = \frac{R - S}{R + S} \quad (1)$$

The number of deflections was defined as the number of local extrema [8]. Deflections of less than 0.5 mV (5% of the amplitude at control) were discarded.

## 3. Results

Along with the progression of microfibrosis, wave-front propagation became more discrete and transverse CV slowed down from 30 cm/s (control) to 7.5 cm/s, as shown in Fig. 2. When  $L$  became closer to the longitudinal space constant (1.2 mm), the propagation of current flow was significantly delayed by the obstacles. Conduction slowing was more pronounced than in a continuous tissue model with random diffuse fibrosis (dashed curve, from [9]).

At control, electrogram amplitude was  $A = 10 \pm 0.2$  mV and their asymmetry was  $a = -0.20 \pm 0.02$  (Fig. 3A). In-

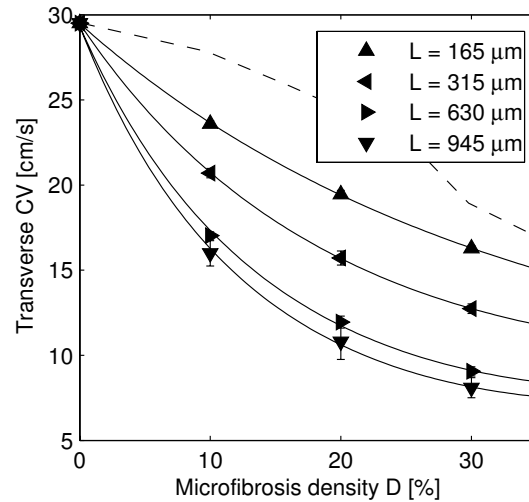


Figure 2. Conduction velocity (CV) for transverse propagation (mean  $\pm$  SD over 6 different tissues) as a function of microfibrosis density ( $D$ ) and average length of collagenous septa ( $L$ ). The dashed line corresponds to the (rescaled) data from ten Tusscher *et al.* [9] (2D continuous tissue model with random diffuse fibrosis).

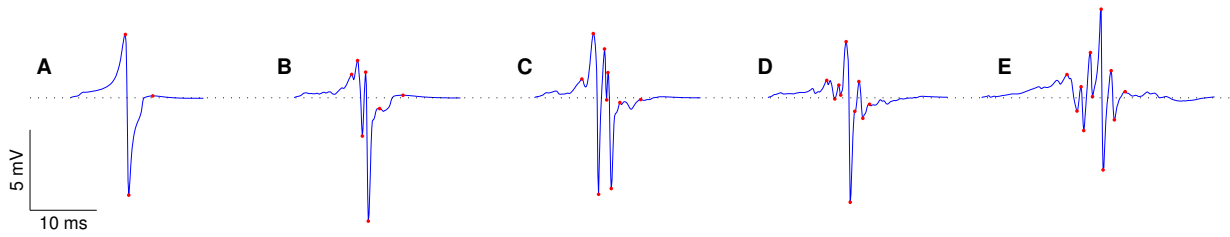


Figure 3. Examples of electrogram waveforms. (A) control; (B)  $D = 10\%$  and  $L = 315 \mu\text{m}$ ; (C)  $D = 10\%$  and  $L = 945 \mu\text{m}$ ; (D)  $D = 30\%$  and  $L = 315 \mu\text{m}$ ; (E)  $D = 30\%$  and  $L = 945 \mu\text{m}$ .

creasing microfibrils density ( $D$ ) reduced average electrogram amplitude down to  $8.84 \pm 1.85 \text{ mV}$  ( $D=10\%$ ),  $7.64 \pm 2.0 \text{ mV}$  ( $D=20\%$ ), and  $6.46 \pm 1.7 \text{ mV}$  ( $D=30\%$ ). Average electrogram amplitude was however not well correlated with CV (correlation coefficient: 0.3).

As the average length ( $L$ ) of collagenous septa was increased, a larger spatial variability in electrogram morphology was observed. The occurrence of positive asymmetric complexes ( $a > 0$ ) was more common for longer  $L$ , as shown in Fig. 4. This reflects the local source-sink mismatch due to the wavefront collision or merging following an obstacle-induced micro-wavebreak [6]. In addition, these micro-wavebreaks caused electrogram fractionation. The average number of deflections was larger for longer  $L$  ( $8.3 \pm 1.0$  for  $L > 500 \mu\text{m}$  vs  $5.7 \pm 1.2$  for  $L < 500 \mu\text{m}$ , 3 at control), indicating a higher degree of fractionation. As a result, electrogram morphology became increasingly more complex when microfibrils was more severe (Fig. 3B–E).

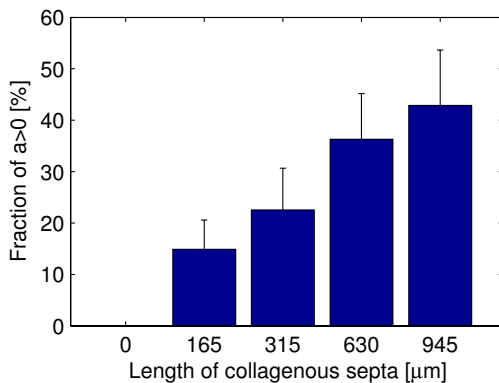


Figure 4. Fraction of positive asymmetric ( $a > 0$ ) electrogram waveforms as a function of the average length of collagenous septa ( $L$ ).

A more detailed quantitative description of electrogram fractionation is presented in Fig. 5. Histograms of the number of deflections are shown for different values of  $L$ . Despite a large spatial variability in the degree of fraction-

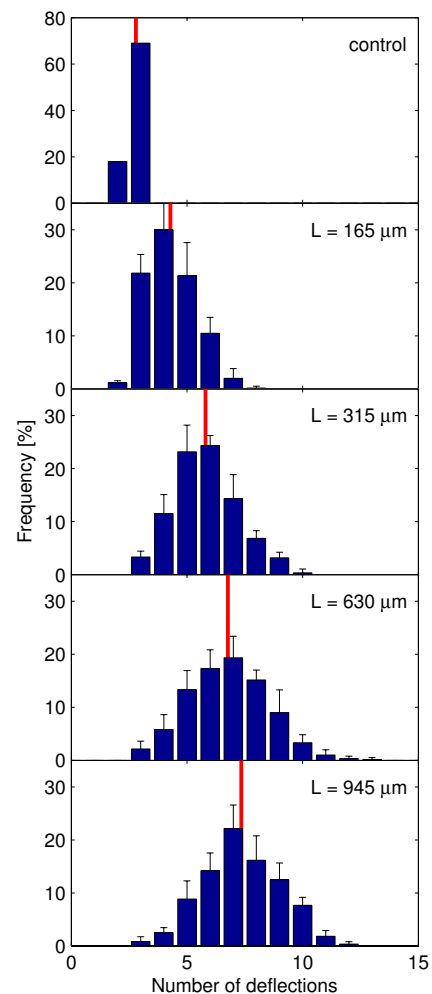


Figure 5. Distribution of the number of deflections for a microfibrils density of  $D = 10\%$  and different lengths of collagenous septa ( $L$ ).

ation, the average number of deflections was consistently higher for larger values of  $L$ .

#### 4. Discussion and conclusions

The results suggest that a higher degree of electrogram fractionation combined with slow conduction indicates a more severe state of microfibrosis, in agreement with Konings *et al.* who observed a larger percentage of fractionated electrograms in zones of slow conduction [10]. The link between substrate properties and degree of electrogram fractionation is however not straightforward. Electrogram morphology depends not only on microfibrosis density ( $D$ ), but also on the length of the collagenous septa ( $L$ ).

Other factors may also affect electrogram fractionation. Macroscale obstacles or abrupt changes in cell coupling can create additional deflections [6, 8] (usually no more than 2 to 4). In the presence of poorly-coupled thin subepicardial layers or endocardial bundles [7], two independent activations may be recorded almost simultaneously at the same site, leading to a longer and more complex waveform. During atrial fibrillation, close to the pivot point of a functional reentry, the occurrence of electrograms with multiple deflections has been reported [10]. For those reasons, substrate mapping is expected to be more accurate when performed during sinus or paced rhythm.

Using the number of deflections for quantifying waveform complexity has some robustness issues. In this paper, electrogram signals were actually extracellular potentials as might be recorded with an ideal point electrode. In clinical applications, the size of the measuring electrode is typically much larger than the microscale obstacles. The spatial averaging effect caused by the electrode may affect the number of deflections. In addition, most of the clinical recordings are bipolar, which could possibly double the number of deflections. The signal-to-noise ratio and the use of a lowpass filter as a preprocessing step are other possible perturbing factors. However, the relatively small number of available standardized catheter electrodes and navigation systems makes it possible to record consistent dataset and ensure reproducibility.

In conclusion, changes in cell-to-cell coupling at the microscale have a significant impact on electrogram morphology. The degree of fractionation of electrograms might be used as a measure to assess the progression of fibrosis. Microstructure computer models may assist the interpretation of electrograms to extract more information about the arrhythmogenic substrate.

#### Acknowledgements

This work was supported by Swiss National Science Foundation Grant PA002-113171 and National Heart,

Lung, and Blood Institute Grant R01 HL-76767.

#### References

- [1] Nademane K, McKenzie J, Kosar E, Schwab M, Sunsaneewitayakul B, Vasavakul Te, Khunnawat C, Ngarmukos T. A new approach for catheter ablation of atrial fibrillation: mapping of the electrophysiologic substrate. *J Am Coll Cardiol* 2004;43(11):2044–53.
- [2] Spach MS, Heidlage JF, Dolber PC, Barr RC. Mechanism of origin of conduction disturbances in aging human atrial bundles: experimental and model study. *Heart Rhythm* 2007;4(2):175–85.
- [3] Jacquemet V, Henriquez CS. Loading effect of fibroblast-myocyte coupling on resting potential, impulse propagation, and repolarization: insights from a microstructure model. *Am J Physiol Heart Circ Physiol* 2008;294(5):H2040–52.
- [4] Hubbard ML, Ying W, Henriquez CS. Effect of gap junction distribution on impulse propagation in a monolayer of myocytes: a model study. *Europace* 2007;9 Suppl 6:vi20–8.
- [5] Ramirez RJ, Nattel S, Courtemanche M. Mathematical analysis of canine atrial action potentials: rate, regional factors, and electrical remodeling. *Am J Physiol Heart Circ Physiol* 2000;279:H1767–85.
- [6] Jacquemet V, Virag N, Ihara Z, Dang L, Blanc O, Zozor S, Vesin JM, Kappenberger L, Henriquez C. Study of unipolar electrogram morphology in a computer model of atrial fibrillation. *J Cardiovasc Electrophysiol* 2003;14(10 Suppl):S172–9.
- [7] Houben RPM, de Groot NMS, Smeets JLRM, Becker AE, Lindemans FW, Allessie MA. S-wave predominance of epicardial electrograms during atrial fibrillation in humans: indirect evidence for a role of the thin subepicardial layer. *Heart Rhythm* 2004;1(6):639–47.
- [8] Lellouche N, Buch E, Celigoj A, Siegeman C, Cesario D, De Diego C, Mahajan A, Boyle NG, Wiener I, Garfinkel A, Shivkumar K. Functional characterization of atrial electrograms in sinus rhythm delineates sites of parasympathetic innervation in patients with paroxysmal atrial fibrillation. *J Am Coll Cardiol* 2007;50(14):1324–31.
- [9] ten Tusscher KHWJ, Panfilov AV. Influence of diffuse fibrosis on wave propagation in human ventricular tissue. *Europace* 2007;9 Suppl 6:vi38–45.
- [10] Konings KT, Smeets JL, Penn OC, Wellens HJ, Allessie MA. Configuration of unipolar atrial electrograms during electrically induced atrial fibrillation in humans. *Circulation* 1997;95(5):1231–41.

Address for correspondence:

Vincent Jacquemet  
136 Hudson Hall, Box 90281  
Durham, NC 27708, USA  
vincent.jacquemet@a3.epfl.ch